Journal of Sound and Vibration (2002) **251**(2), 373–376
doi:10.1006/jsvi.2001.3820, available online at http://www.idealibrary.com on IDEAL®

PITCHFORK PHASE "BIFURCATION" OF ISOLATOR STIFFNESS

L. Kari

MWL/Department of Vehicle Engineering, Kungliga Tekniska Högskolan, 100 44 *Stockholm, Sweden.*
E-mail: leifk@fkt.kth.se

(*Received* 6 *April* 2001)

Referring to a recently presented waveguide model [1, 2] the dependence of the dynamic stiffness on the radius and length of cylindrical vibration isolators can be determined. It constitutes a major practical application; in particular, predicting the dynamic stiffness alteration due to change in geometry of a given isolator. While changing the geometry it is, for example, found that the dynamic stiffness curve, in general, shifts to higher frequencies as the isolator shortens and that the magnitude of the peaks increases sharply with increased isolator radius. This is not surprising, but this is: some stiffness peaks move along the frequency axis while changing the radius; occasionally, peaks and troughs develop or disappear while changing the radius or length, and, finally, the stiffness phase, sporadically, jumps as the isolator radius or length alters. The latter, interesting phenomenon is illustrated in this Letter.

Consider the cylindrical vibration isolator in Figure 1, length L and radius R, made of rubber with density ρ and equipped with bonded circular steel plates. The isolator is excited at one end, while being blocked; that is, zero displacement, at the opposite end. The blocked dynamic driving point and transfer stiffnesses are defined as $\tilde{k}_D = \tilde{f}_{in}/\tilde{u}_{in}$ and $\tilde{k}_T = \tilde{f}_{out}/\tilde{u}_{in}$, respectively, where u is the displacement, f is the force and $\tilde{(\cdot)} = \int_{-\infty}^{\infty}(\cdot)\exp(-\mathrm{i}\omega t)\,\mathrm{d}t$ is the temporal Fourier transformation with i denoting the imaginary unit, ω the angular frequency and t the time. The shear modulus of rubber is modelled as a fractional Kelvin–Voigt model [3]

$$\hat{\mu}(\omega) = \mu_\infty \left[1 + \left(\frac{\mu_v}{\mu_\infty}\,\mathrm{i}\omega\right)^\alpha\right], \tag{1}$$

where the equilibrium shear modulus $\mu_\infty = 5{\cdot}9355 \times 10^5\ \mathrm{N/m^2}$; $\alpha = 2{\cdot}9700 \times 10^{-1}$ and $\mu_v = 5{\cdot}9944\ \mathrm{Ns/m^2}$. The resulting shear modulus in Figure 2 is typical for a crosslinked rubber; its magnitude and loss factor increase slightly with frequency within the considered frequency range 0–1000 Hz. Moreover, the rubber is assumed to be nearly incompressible with compression relaxation function κ and equilibrium shear modulus being dependent as $\kappa(t) = b\mu_\infty h(t)$, where the material constant $b = 2{\cdot}2220 \times 10^3$ and h is a step function, resulting in a constant bulk modulus $1{\cdot}3189 \times 10^9\ \mathrm{N/m^2}$ and the equilibrium Poisson ratio $4{\cdot}9978 \times 10^{-1}$. The waveguide theory relies upon the dispersion relations for an infinite cylinder, already developed by Pochhammer [4] and Chree [5] in the 19th century, where the axial dependence is separated and the eigenvalues and eigenmodes of the cross-section are calculated. The total field is then obtained by eigenmode superposition while matching them to the cylinder end boundary conditions.

0022-460X/02/120373 + 04 $35.00/0

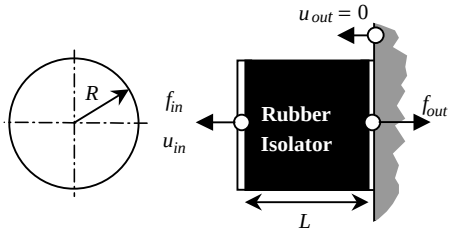

Figure 1. Vibration isolator and exposed junction variables including the blocking force.

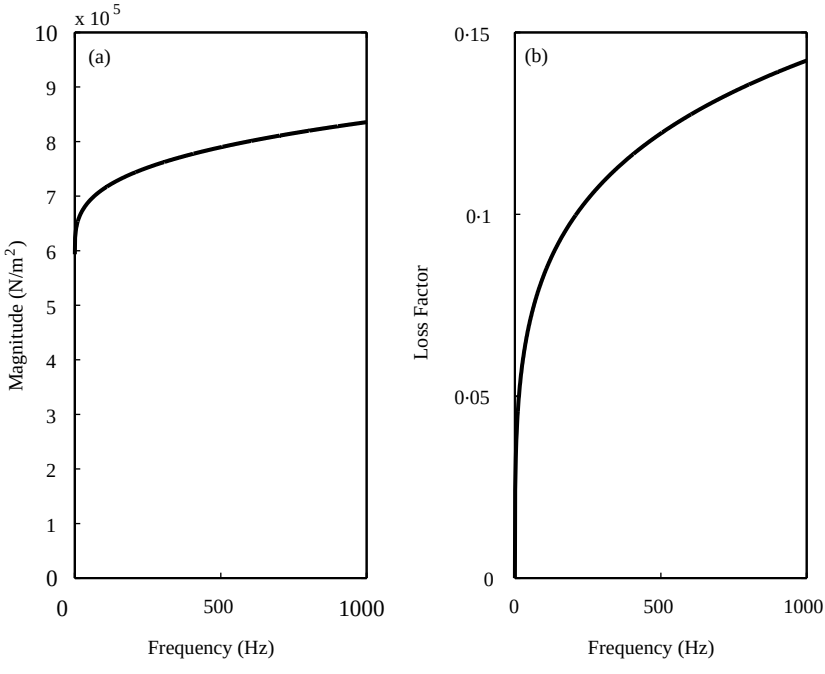

Figure 2. Shear modulus magnitude $|\hat{\mu}|$ and loss factor Imag $\hat{\mu}$/Real $\hat{\mu}$ versus frequency.

The transfer stiffness, in the narrow frequency band 723–733 Hz, is in Figure 3 for an isolator with $\rho = 1{\cdot}0500 \times 10^3\,\mathrm{kg/m^3}$, $R = 5{\cdot}0000 \times 10^{-2}\,\mathrm{m}$ and $L = L_0 \pm nL_\varepsilon$, where $L_0 \approx 5{\cdot}757 \times 10^{-2}\,\mathrm{m}$, $L_\varepsilon = 0{\cdot}5\,\mu\mathrm{m}$ and $n = 1{,}100$. The curves corresponding to $L = L_0 + L_\varepsilon$, $L_0 - L_\varepsilon$, $L_0 + 100L_\varepsilon$ and $L_0 - 100L_\varepsilon$ are plotted in solid, dotted, dashed and dash–dotted lines respectively. The stiffness phase curve is displayed unwrapped with respect to phase starting at 0 Hz.

Clearly, the solid and dotted phase curves jump instantaneously $\pm 180^\circ$ at $f_0 \approx 728{\cdot}4$ Hz as the isolator length alters 1 μm only; the -180° jump may be interpretable as a complex mode pattern governed antiresonance, while the $+180^\circ$ jump as a resonance. The ensuing phase difference is, however, $\sim 360^\circ$; thus, resulting in a subsequent (wrapped) stiffness phase coincidence. The number of eigenmodes applied in this analysis is large; namely 256 (128 with positive and 128 with negative real-part eigenvalues). The overall stiffness difference between this solution and a solution with more eigenmodes, for example 512, is negligible ($f_0^{256} = 728{\cdot}41$ Hz, $L_0^{256} = 5{\cdot}7573 \times 10^{-2}\,\mathrm{m}$; $f_0^{512} = 728{\cdot}48$ Hz, $L_0^{512} = 5{\cdot}7565 \times 10^{-2}\,\mathrm{m}$); thus, verifying the waveguide solution convergence. The sharp pitchfork phase

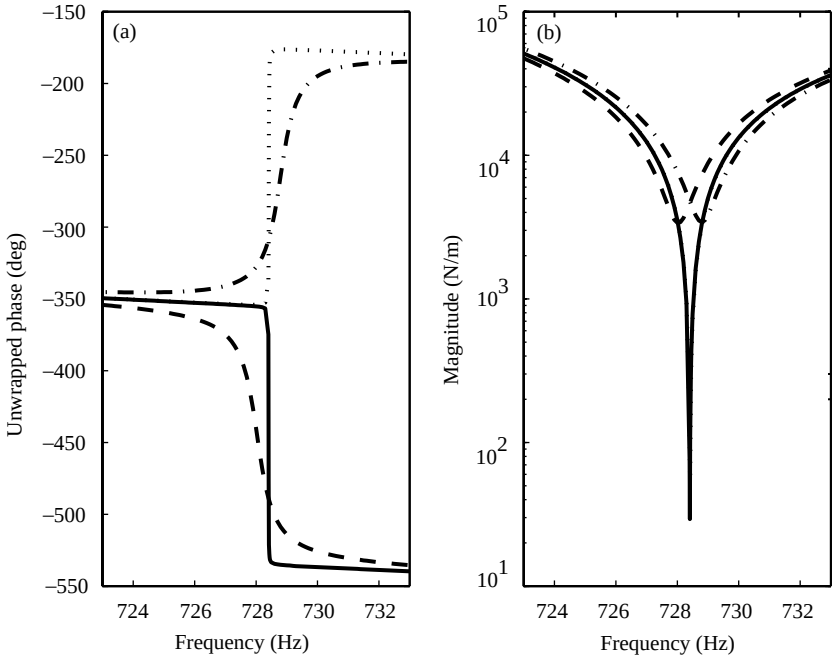

Figure 3. Dynamic transfer stiffness in a narrow frequency band of 723–733 Hz. Length: $L = L_0 + L_\varepsilon$ (solid), $L_0 - L_\varepsilon$ (dotted), $L_0 + 100L_\varepsilon$ (dashed) and $L_0 - 100L_\varepsilon$ (dash–dotted), where $L_0 \approx 5{\cdot}757 \times 10^{-2}$ m and $L_\varepsilon = 0{\cdot}5\,\mu$m.

"bifurcation" curve is smoothed as the length difference increases; this is clearly illustrated in Figure 3 by the dashed and dash–dotted phase curves representing an isolator length difference of 0·1 mm.

Next, the transfer stiffness magnitude is studied. The solid and dotted magnitude curves to the right in Figure 3, representing an isolator length difference of 1 μm, almost coincide while developing a deep, sharp trough at f_0. In theory, $\lim \tilde{k}_T(f, L) = 0$ as $f, L \to f_0, L_0$, while the "half-power bandwidth" Δf_0 of the trough shrinks to zero; surprisingly, as the shear modulus loss factor of the rubber is approximately 13% at f_0 in Figure 2. Consequently, large errors may be introduced using $\triangle f_0/f_0$ of a stiffness trough, as a measure of material damping. Sharp, deep stiffness magnitude troughs in connection with phase jumps are also detected in rubber isolator measurements [6] and in finite elements analysis—the author to this Letter verifying the phenomenon—using the method presented in reference [7]. What about driving point stiffness behavior? The deep, sharp magnitude troughs and sudden phase jumps disappear; not surprising as $0 \leqslant \angle\, \tilde{k}_D \leqslant 180^\circ$ on physical grounds; thus, forcing the driving point resonance and anti-resonance order to be consecutive.

In summary, the transfer stiffness is found to occasionally develop a deep, narrow magnitude trough with a sudden phase jump while changing the isolator length or radius. The method applied is a newly developed waveguide model where the rubber is modelled as nearly incompressible with deviatoric viscoelasticity based on a fractional order derivative model. The main advantage of the fractional Kelvin–Voigt model is the small parameter number required to successfully model the material properties over a broad structure-borne sound frequency domain. However, the sudden phase jumps and sharp magnitude drops for the driving point stiffness, disappear as the resonances and anti-resonances are required to alternate.

REFERENCES

1. L. KARI 2001 *Journal of Sound and Vibration* **244**, 211–233. On the waveguide modelling of dynamic stiffness of cylindrical vibration isolators. Part I: the model, solution and experimental comparison (jsvi.2000.3468).
2. L. KARI 2001 *Journal of Sound and Vibration* **244**, 235–257. On the waveguide modelling of dynamic stiffness of cylindrical vibration isolators. Part II: the dispersion relation solution, convergence analysis and comparison with simple models (jsvi.2000.3469).
3. R. C. KOELLER 1984 *Journal of Applied Mechanics, Transactions of the American Society of Mechanical Engineers* **51**, 299–307. Applications of fractional calculus to the theory of viscoelasticity.
4. L. POCHHAMMER 1876 *Journal für die reine und angewandte Mathematik* **81**, 324–336. Über die Fortpflanzungsgeschwindigkeiten kleiner Schwingungen in einem unbegrenzten isotropen Kreiszylinder.
5. C. CHREE 1889 *Transactions of the Cambridge Philosophical Society* **14**, 250–369. The equations of an isotropic elastic solid in polar and cylindrical coordinates, their solutions and applications.
6. L. KARI 2001 *Noise Control Engineering Journal* **49**, 88–102. Dynamic transfer stiffness measurements of vibration isolators in the audible frequency range.
7. L. KARI 1999 *Proceedings, Sixth International Congress on Sound and Vibration*, vol. 5, 2081–2090. The audible stiffness of preloaded vibration isolators.